Organic Electronics 13 (2012) 550–559

Contents lists available at SciVerse ScienceDirect

Organic Electronics

journal homepage: www.elsevier.com/locate/orgel

Effect of residual catalyst on solar cells made of a fluorene-thiophene-benzothiadiazole copolymer as electron-donor: A combined electrical and photophysical study

Nadia Camaioni [a,*], Francesca Tinti [a], Lorenzo Franco [b], Marianna Fabris [b], Antonio Toffoletti [b], Marco Ruzzi [b], Luciano Montanari [c], Lucia Bonoldi [c], Andrea Pellegrino [d], Anna Calabrese [d], Riccardo Po [d,*]

[a] Istituto per la Sintesi Organica e la Fotoreattività, Consiglio Nazionale delle Ricerche, via P. Gobetti 101, I-40129 Bologna, Italy
[b] Dipartimento di Scienze Chimiche, Università di Padova, via Marzolo 1, 35131 Padova, Italy
[c] Centro Ricerche Divisione Refining and Marketing, ENI S.p.A, via Maritano 26, 20097 San Donato Milanese, Italy
[d] Centro Ricerche per le Energie non Convenzionali, Istituto ENI-Donegani, ENI S.p.A., via Fauser 4, 28100 Novara, Italy

ARTICLE INFO

Article history:
Received 30 September 2011
Received in revised form 30 November 2011
Accepted 11 December 2011
Available online 10 January 2012

Keywords:
Palladium catalyst
Charge transport
Trap states
Electron Spin Resonance
Solar cells

ABSTRACT

The effects of residual catalyst impurities (palladium) on the hole mobility of a fluorene-thiophene-benzothiadiazole copolymer (poly{[4′-(9,9-bis(2-ethylhexyl)fluoren-2-yl)-2′,1′,3′-benzothiadiazole-7,7′-diyl]-co-[2′-(9,9-bis(2-ethylhexyl)fluoren-2-yl)thien-7,5′-diyl]}) (PFB-co-FT), as well as on its photovoltaic and photophysical response when blended with [6,6]-phenyl-C_{61}-butyric acid methyl ester (PCBM), are investigated. Two samples of the copolymer, only differing for the Pd content (9 and 3360 ppm), are considered and compared. The transport of positive carriers is characterized by a lower mobility and a higher dispersion in the Pd-rich PFB-co-FT sample. The photovoltaic parameters of PFB-co-FT:PCBM solar cells show a significant dependence on the residual catalyst impurities, attributed to a different concentration of trap states. Variations in charge mobility and trapping induced by impurities was confirmed also by ESR (Electron Spin Resonance) experiments: an increased concentration of trapped charges in the presence of a higher level of metal impurities was revealed by light induced ESR, while the variation of polaron mobility correlates with the lifetime variation of the photogenerated PCBM triplet state detected by time-resolved ESR. All experimental evidences point to a strong effect of Pd impurities on the transport properties of charge carriers.

1. Introduction

The performance of the so-called bulk-heterojunction (BHJ) solar cells [1], made of an interpenetrated network of a conjugated polymer as electron-donor (D) and a soluble fullerene derivative as electron-acceptor (A), underwent to a significant improvement during the recent years. This has been mainly achieved by the combination of improved material engineering [2] and fine control of the nanoscale morphology of the D/A blend [3]. Following the approach of the energy level engineering, novel donor materials with enhanced electronic properties have been prepared, leading to solar cell with efficiencies exceeding 8% [4]. To further improve the power conversion efficiency of BHJ polymer/fullerene solar cells, much efforts are required to understand the factors limiting the device performance and, among them, the transport properties of charge carriers in the interpenetrated D/A blends are attracting greater and greater attention with respect to the past [5].

* Corresponding authors.
E-mail addresses: camaioni@isof.cnr.it (N. Camaioni), riccardo.po@eni.com (R. Po).

1566-1199/$ - see front matter © 2011 Elsevier B.V. All rights reserved.
doi:10.1016/j.orgel.2011.12.005

Fullerene derivatives commonly employed as acceptors in BHJ solar cells are characterized by a high mobility of negative carriers and values of the order of 10^{-3} cm^2 V^{-1} s^{-1} are usually reported in optimized polymer/fullerene blends [6]. Thus, transport properties in this kind of solar cells are mainly limited by the poor mobility of positive carriers in the polymer phase, typically of 10^{-6}–10^{-5} cm^2 V^{-1} s^{-1} [7], leading to an unbalanced charge transport. It has been clearly demonstrated that high and balanced mobilities are a prerequisite for efficient polymer/fullerene solar cells, (i) to avoid space charge effects [8], (ii) to reduce the occurrence of recombination processes [9], (iii) not to limit solar light harvesting by the use of too thin photoactive layers [10].

Charge transport in conjugated polymer films takes place by hopping through a manifold of localized states [11], so carrier mobility is intrinsically low for this kind of materials and affected by a lot of parameters. Apart from charge delocalization, factors such as molecular weight, regioregularity, position and nature of the side-chain groups, as well as chemical purity play a relevant role for charge transport properties of conjugated polymer films [12].

One of the main sources of chemical impurities is represented by residual catalyst used in the polymerization process, affected by the method of polymer preparation as well as by the purification process. Worth noticing, most of donor polymer currently used in highly efficient solar cells are obtained through palladium catalyzed polycondensations [13]. In the palladium-catalyzed polymerizations (Suzuki, Stille, Heck, Sonogashira, etc.), and, in general, in most of the methods used for the synthesis of conjugated polymers, the metal catalysts can be strongly coordinated by the heteroatoms present on the polymer backbone, so that their removal is difficult, other than time-consuming, and sometimes involves extremely toxic chemicals (cyanides). It has also been reported that insoluble metallic nanoparticles are formed in some cases [14,15] contaminating the polymer and affecting its electronic properties. A variation of orders of magnitude has been reported for the field-effect mobility measured for poly(3-hexylthiophene) (P3HT) polymer samples, prepared by oxidative coupling using ferric chloride and purified to different extents [16]. Differently, other studies have shown that the performance of field-effect transistors, made with other conjugated polymers with different levels of metal contamination (Fe, Pd, Zn, Sn), are not meaningfully affected by the impurity level [17,18], though a higher hysteresis has been observed for higher Pd content [17]. In a couple of recent works, it has been shown how hole mobility decreases in P3HT with increasing palladium content, according to impedance measurements [19], and how the performance of related devices is affected [20]. Although the authors themselves are aware that "artificial" impurities differ significantly from those present in real systems, the investigated polymer samples were prepared by intentionally adding known amounts of the palladium catalyst precursor ($Pd[PPh_3]_4$) to P3HT. However, according to Krebs et al. [14] the residual palladium from Heck polycondensation in a polyphenylenevinylene is present in the final polymer in the form of metallic nanoaggregates. Moreover, it should also be noted that the typical metal impurities of P3HT are nickel and zinc, not palladium, because P3HT is routinely prepared through Kumada, McCullough or Rieke polymerizations [21]. Only in a recent paper [22] the variation of the performance of poly[4,4-bis(2-ethylhexyl)-4Hcyclopenta[2,1-b;3,4-b′]dithiophene-2,6-diyl-alt-2,1,3-benzothiadiazole-4,7-diyl]:PCBM solar cells (PCBM is methyl [6,6]-phenyl-C_{61}-butyrate) with the polymer purity has been reported. In that work the chemical impurities were those arising from the original catalyst and monomers, but the Pd content was not accurately quantified because of the detection limit of the measurement system (3000 ppm) [22].

Although the utmost importance of charge transport properties for polymer electronics and in particular for polymer solar cells, the effect of impurities on the performance on these devices has been poorly reported in the literature. In this study, the effect of Pd catalyst impurities – even at low levels – on the properties of a fluorene-thiophene-benzothiadiazole copolymer, poly{[4′-(9,9-bis(2-ethylhexyl)fluoren-2-yl)-2′,1′,3′-benzothiadiazole-7,7′-diyl]-co-[2′-(9,9-bis(2-ethylhexyl)fluoren-2-yl)thien-7,5′-diyl]} (PFB-co-FT, Fig. 1) are investigated. To this end, two samples of PFB-co-FT were prepared by removing the catalyst residues from a common copolymer precursor, so the palladium present in the investigated polymer samples was not artificially introduced but derived from the synthetic process. The variation induced by the Pd residual impurities in the bulk transport properties of PFB-co-FT films as well as in the photovoltaic behaviour of PFB-co-FT:PCBM solar cells are reported and discussed. In addition, light induced Electron Spin Resonance (ESR) and time-resolved

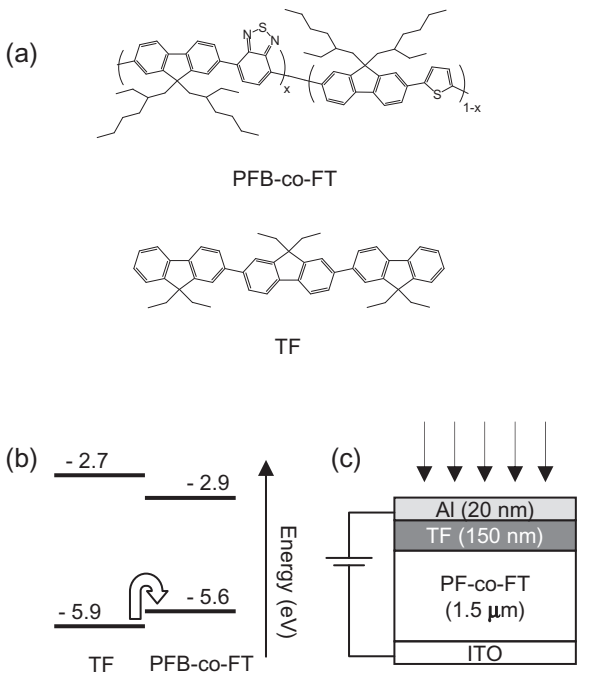

Fig. 1. (a) Molecular structures of materials used in this study; (b) energy levels diagram; (c) the device structure used for Time-of-Flight measurements.

ESR (TRESR) with sub-microseconds time resolution, in combination with visible light excitation, are used to reveal the effect of Pd impurities on the photoexcited species lifetime in PFB-co-FT:PCBM blends.

The results here reported show a clear dependence of hole mobility of PFB-co-FT on the residual Pd impurities and a significant variation of the photovoltaic parameters of PFB-co-FT:PCBM solar cells, prepared with polymer samples with different Pd contents. Similarly, differences were found in the ESR spectra of PFB-co-FT:PCBM blends, with intensities dependent on the copolymer purity, either in steady-state or in transient mode. The experimental evidences are discussed in terms of different trap states distributions created by the residual Pd catalyst.

2. Experimental

2.1. Materials

Poly{[4′-(9,9-bis(2-ethylhexyl)fluoren-2-yl)-2′,1′,3′-benzothiadiazole-7,7′-diyl]-co-[2′-(9,9-bis(2-ethylhexyl)fluoren-2-yl)thien-7,5′-diyl]} has been prepared as reported elsewhere [23] by Suzuki polycondensation of boronic acid of fluorene derivative, dibromobenzothiadiazole and 2,5-dibromothiophene catalyzed by $Pd[PPh_3]_4$. The product obtained from the polymerization was identified as PFB-co-FT_A. A portion of the polymer was dissolved in 500 mL of chloroform and 500 mL of 30% aqueous ammonia were added. The mixture was vigorously stirred for 3 h at reflux temperature and cooled to room temperature. The organic phase was separated, 400 mg of disodium ethylenediaminetetraacetate were added and the mixture was stirred overnight. Then the suspension was extracted three times with 500 mL of water. The organic phase was separated, concentrated to about 10 mL and added dropwise to 200 mL of methanol to precipitate the polymer. The solid was collected by filtration, washed with methanol and dried in a vacuum oven to yield PFB-co-FT_B. Palladium content in the two polymer samples, determined by ICP-mass analysis with a Perkin Elmer Elan DRC-e spectrometer, was found to be 3360 and 9 ppm (w/w), for PFB-co-FT_A and PFB-co-FT_B respectively.

2.2. TOF measurements

PFB-co-FT films were spin-coated onto glass/ITO (Indium–Tin-Oxide) substrates from chloroform solutions to a thickness of about 1.50 μm. A 150-nm thick layer of terfluorene was vacuum evaporated on the top of the PFB-co-FT films, as a charge generation layer. The device structure was completed with a vacuum evaporated semi-transparent aluminium electrode (20 nm), acting as the illuminated electrode. A nitrogen laser ($\lambda = 337$ nm) with a pulse duration of 6–7 ns was used to photogenerate charge carriers. A variable DC potential, with the Al electrode positively biased, was applied to the samples and, in order to ensure a uniform electric field inside the device, the total photogenerated charge was kept less than 0.1 CV, where C is the sample capacitance and V the applied potential. The photocurrent was monitored across a variable load resistance by using a Tektronix TDS620A digital oscilloscope.

2.3. Solar cells

Solar cells were fabricated on patterned ITO-coated glass substrates previously cleaned in detergent and water, then ultrasonicated in acetone and isopropyl alcohol for 15 min each. A PEDOT:PSS (Clevios P VP AI 4083) layer was spin-coated at 4000 rpm onto UV–ozone-treated ITO-coated substrates to a thickness of around 40 nm, then baked in an oven at 140 °C for 10 min. PFB-co-FT was blended with PCBM (Aldrich) and dissolved in 1,2-dichlorobenzene (25 g L^{-1}). The solutions were stirred at 40 °C for 4 days. The blend solutions were spin-coated in air onto the ITO/PEDOT:PSS substrates. The thickness of the active layers, measured with a Tencor AlphaStep profilometer, was around 100 nm. Then the samples were transferred to an argon glove-box, where the device structure was completed with the thermal evaporation of the LiF (0.9 nm)/Al (80 nm) cathode at a base pressure of 3×10^{-6} mbar. The active device area, defined by the shadow mask used for the cathode deposition, was 8 mm^2.

The device electrical characterization was carried out at room temperature in an argon glove-box. Solar cells were illuminated by using a solar simulator (SUN 2000 Abet Technologies, AM1.5G) and the light power intensity was calibrated using a certified silicon solar cell. For light-intensity dependent measurements, a set of quartz neutral filters was used to vary the incident light power. The current–voltage curves were taken with a Keithley 2400 source-measure unit.

2.4. Light induced ESR and TRESR Spectroscopy

ESR spectra were recorded with a Bruker Elexsys E500 X-band spectrometer (9–10 GHz working frequency) equipped with a nitrogen flow cryostat for sample temperature control (110–400 K). Light induced ESR spectra were obtained by subtracting the ESR spectrum recorded in the dark from the spectrum recorded under illumination. Light excitation was obtained using either the IR-filtered output of a high pressure Xe lamp (≈1 mW cm^{-2} on the sample) or a laser excitation (from an Argon Neon laser, emitting at 488 nm and 514 nm, ≈40 mW cm^{-2} on the sample). The two irradiation methods gave similar results.

For ESR spectra, PFB-co-FT:PCBM films were obtained from mixed solution of polymer and fullerene in 1,2-dichlorobenzene (1:1 by weight, at 1 g L^{-1}); films 2 cm high are prepared putting a fixed appropriate quantity of solution inside ESR quartz tubes (4 mm outer diameter) and slowly evaporating the solvent under vacuum after three freeze–pump–thaw cycles; after a successive 2 h vacuum treatment the tubes are sealed and the films analysed; minor differences of volume are measured and accounted for. We took care to maintain the same geometrical setup (position of sample tubes in the resonant cavity) in all the measurement. The small dimensions of the weighted sample allow to put it inside the region of the resonant cavity giving a constant instrumental response. At fixed illumination conditions, these cares allow to have

a good repeatability and to compare quantitatively the LESR intensities. Indeed repeated measurement on independently prepared samples showed a variation on LESR response of less than 15%.

TRESR experiments in the microsecond time range were performed with a Bruker ER200D ESR spectrometer, and photoexciting the sample with the second harmonic of a Nd:YAG pulsed laser (Quantel Brilliant, $\lambda = 532$ nm; 5 ns pulse duration; energy/pulse ≅5 mJ, 20 Hz repetition rate). By disabling magnetic field modulation, positive and negative TRESR intensities indicate absorptive and emissive lines, respectively. The overall response time of the instrument was about 150 ns. At each magnetic field position, an average of 200 transients is usually recorded and a 2D data-set was obtained, giving either the ESR spectrum at different time delays after the laser pulse or the ESR signal time evolution at each magnetic field position. Sample preparation for TRESR experiments was the same as for LESR. All geometrical (sample volume and position), optical (laser light intensity and sample area excited by the laser) and instrumental parameters have been kept as constant as possible. Repeated measurement on independently prepared samples showed a variation on TRESR response of less than 10%.

3. Results and discussion

The two investigated copolymer samples were indentified as PFB-co-FT_A and PFB-co-FT_B. The former was directly obtained by Suzuki cross-coupling polymerization with ($Pd[PPh_3]_4$) catalyst, the latter was achieved after a purification process. The two PFB-co-FT samples were thoroughly characterized in order to exclude any other difference, besides the content of the residual palladium (3360 and 9 ppm for PFB-co-FT_A and PFB-co-FT_B, respectively) and phosphorus catalyst (800 and 670 ppm for PFB-co-FT_A and PFB-co-FT_B, respectively). Since phosphorus content is not significantly different in the two samples, any variation is mainly attributed to palladium. NMR and UV–vis absorption spectra were found to be exactly coincident. Solubility, molecular weights and their distribution, as well as the energy levels of the highest occupied molecular orbital (HOMO) and of the lowest unoccupied molecular orbital (LUMO) (Table 1) do not significantly differ for the two copolymer samples and are in any case within the experimental error (see Supplementary Data for details).

The bulk transport properties of positive carriers in PFB-co-FT films were investigated by small-signal Time-of-Flight (TOF) [24]. The TOF measurements were performed at room temperature by using the device structure ITO/PFB-co-FT/terfluorene/Al shown in Fig. 1. The thin layer of terfluorene (TF, Fig. 1) acts as a charge generation layer (CGL) [25]. Indeed, because of the high absorption coefficient of TF at the excitation wavelength of the TOF equipment (around $1.3 \times 10^5\ cm^{-1}$ at 337 nm) [26], the thin CGL layer is able to efficiently absorb the incident light pulse. In addition, thanks to its deep-lying HOMO level [24], the holes photogenerated in the CGL (with the illuminated semitransparent Al electrode positively biased) are easily injected into the PFB-co-FT film, as illustrated in Fig. 1.

The photocurrent signals were found to be extremely dispersive, for both PFB-co-FT formulations. A typical photocurrent transient is displayed in Fig. 2 in a double logarithmic scale, while in the inset the same signal is shown in a linear scale. The photocurrent signal shown in Fig. 2 was obtained for PFB-co-FT_A at DC bias of 90 V, corresponding to an electric field E of around $6.1 \times 10^5\ V\ cm^{-1}$. The transit times t_t were extracted from the inflection points in the double logarithmic plots, thus the hole mobility μ was calculated through the well-known expression $\mu = d/t_t E$ where d is the thickness of the PFB-co-FT film. Actually, the time required for holes to cross the charge generation layer should be subtracted from the values of t_t extracted from the photocurrent signals. However, given the high hole mobility of TF (around $1 \times 10^{-3}\ cm^2\ V^{-1}\ s^{-1}$ at $2.5 \times 10^5\ V\ cm^{-1}$) [26] and the small thickness of the terfluorene layer, the transit time of carriers through the CGL was not taken into account.

The mobility values are reported as a function of the square root of E in Fig. 3. As expected, μ is clearly affected by the residual Pd content in the polymer. PFB-co-FT_B exhibits hole mobilities roughly four-fold higher, compared to PFB-co-FT_A with a higher amount of residual catalyst. For example, at a field of around $5 \times 10^5\ V\ cm^{-1}$, hole mobility calculated for PFB-co-FT_A is $3.9 \times 10^{-5}\ cm^2\ V^{-1}\ s^{-1}$, while that of PFB-co-FT_B is $1.6 \times 10^{-4}\ cm^2\ V^{-1}\ s^{-1}$. The trend of mobility with $E^{1/2}$ is roughly linear, suggesting that mobility in PFB-co-FT obeys, in the investigated range of field, a Poole–Frenkel behavior [27,28].

$$\mu(E) = \mu_0 \exp(\beta\sqrt{E}) \tag{1}$$

where μ_0 denotes the mobility at zero field and β is the parameter describing how strong is the dependence on the electric field. The parameters for the Poole–Frenkel fit to mobility data of Fig. 3 are $\mu_0 = 9.4 \times 10^{-7}\ cm^2\ V^{-1}\ s^{-1}$ and $\beta = 5.2 \times 10^{-3}\ (cm\ V^{-1})^{1/2}$, for PFB-co-FT_A, are $\mu_0 = 3.6 \times 10^{-6}\ cm^2\ V^{-1}\ s^{-1}$ and $\beta = 5.3 \times 10^{-3}\ (cm\ V^{-1})^{1/2}$, for PFB-co-FT_B.

The square root field dependence of mobility, frequently observed in disordered molecular materials [29] is often attributed to trapping effects. The immobilization of carriers for time periods by trapping sites distributed in energy leads to a broad distribution of transit times, that

Table 1
Properties of PFB-co-FT polymer samples and charge transport parameters.

Polymer sample	Polymer properties						Transport parameters		
	Pd (ppm)	P (ppm)	Mw (Da)	PDI	HOMO (eV)	LUMO (eV)	μ_0 ($cm^2\ V^{-1}\ s^{-1}$)	β ($cm^{1/2}\ V^{-1/2}$)	α
PFB-co-FT_A	3360	800	31,400	2.95	−5.31	−2.93	9.4×10^{-7}	5.2×10^{-3}	0.32
PFB-co-FT_B	9	670	33,600	2.95	−5.31	−2.94	3.6×10^{-6}	5.3×10^{-3}	0.42

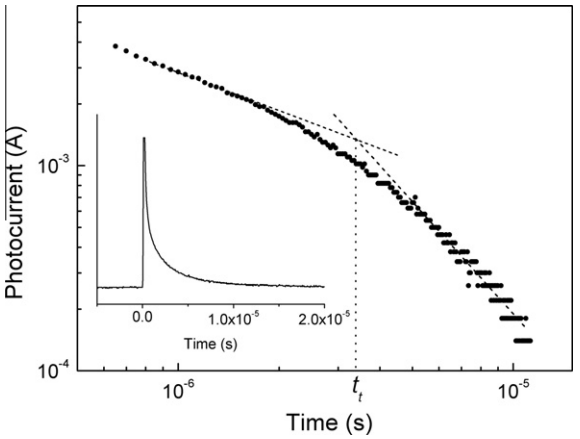

Fig. 2. Photocurrent transient for a device based on PFB-co-FT_A, for an applied bias of 90 V. The thickness of the polymer layer was 1.50 μm.

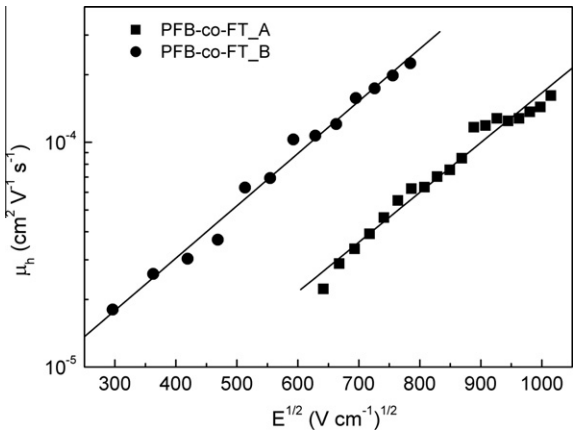

Fig. 3. Square root field dependence of hole mobility for devices based on PFB-co-FT_A (squares) and on PFB-co-FT_B (circles). The lines represent the linear fit to the experimental data.

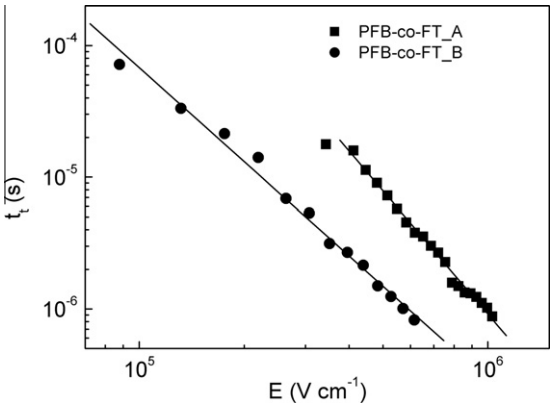

Fig. 4. Electric field dependence of hole transit times for devices based on PFB-co-FT_A (squares) and PFB-co-FT_B (circles). The lines represent the linear fit to the experimental data.

is to a dispersive transport. It has been shown [30] that, in a multiple trapping model, the transit time of carriers exhibits the electric field dependence of $t_t(E) \propto E^{-1/\alpha}$, where α is a dispersion parameter ($0 < \alpha < 1$; $\alpha = 1$ for non dispersive transport) introduced by Scher and Montroll [31] in their model for the description of dispersive transport in amorphous solids. The electric field dependence of hole transit times derived from the TOF signals are reported in Fig. 4 in a double logarithmic plot. From the slopes of the lines representing the linear fit to the experimental data, values for the dispersion parameter α of 0.32 and 0.42 were obtained, for PFB-co-FT_A and PFB-co-FT_B, respectively. So, the residual impurities seem to increase the dispersive character of hole transport, other than affecting the mobility values. The charge transport parameters obtained for PFB-co-FT samples are summarized in Table 1.

In order to analyze the effect of Pd content on the photovoltaic properties of PFB-co-FT, BHJ solar cells were prepared with the two polymer samples as donors and PCBM as acceptor. The device behaviour was investigated by varying the donor to acceptor weight ratio (D:A) of the active layer. For a better comparison, the same experimental conditions were used (same solvent and solution concentration, same spin-coater revolution speed, same active layer thickness), in order to achieve a comparable morphology for PFB-co-FT:PCBM blends made with the same D:A ratio. A remarkable effect was observed for the open-circuit voltage (V_{oc}) and fill factor (FF) of cells made with the different donor samples, reflecting in the power conversion efficiency (PCE), whereas a less significant effect was obtained for the short-circuit current (J_{sc}) (Fig. 5). As shown in Fig. 5, in which the average values of the photovoltaic parameters (over eight cells) are compared by varying the D:A ratio for a comparable thickness of the active layer (around 100 nm), both V_{oc} and FF are significantly lower for cells made with PFB-co-FT_A, translating in a factor of about two in the overall cell efficiency. For both donors, the highest overall performance was achieved for the D:A ratio of 1:2. As expected, because of the high energy gap (about 2.7 eV) of the absorbing polymer, PCE is modest for these cells (0.14% and 0.25% at 100 mW cm^{-2} for PFB-co-FT_A and PFB-co-FT_B, respectively). However, the relevant result here is the relative variation of the photovoltaic parameters and not the absolute values, which, in terms of efficiency, means a variation close to 80% for the investigated cells.

By changing the weight concentration of PCBM between 50% and 75%, the average value of V_{oc} ranged between 0.54 and 0.64 V and between 0.93 and 0.98 V for PFB-co-FT_A and PFB-co-FT_B, respectively. This significant variation with the polymer sample is not expected on the basis of the energy levels of the D/A couple [32], the HOMO level of the donor polymer being not meaningfully affected by the Pd content (Table 1). Also the fill factor was systematically lower for the cells made with the Pd-rich polymer sample, showing its greatest variation at the best D:A ratio (0.33 and 0.42 for PFB-co-FT_A and PFB-co-FT_B, respectively, at D:A of 1:2). The strong effect of the impurity content in the donor polymer on both V_{oc} and FF, could be a signature of trapping effects and, in this case, also a

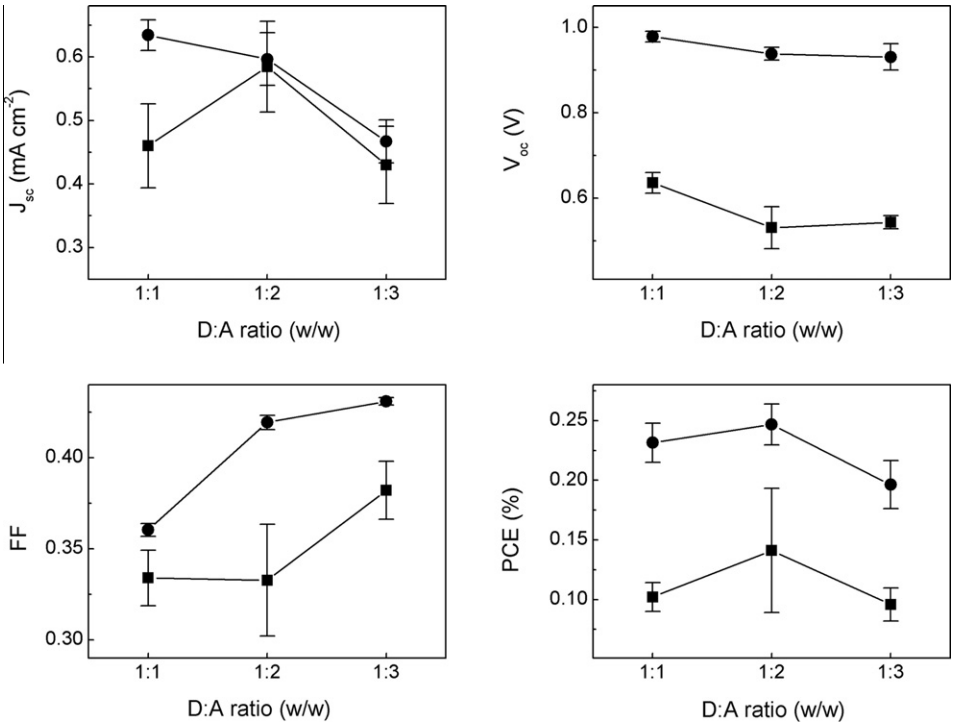

Fig. 5. Dependence of photovoltaic parameters on the donor to acceptor weight ratio for PFB-co-FT_A:PCBM (squares) and PFB-co-FT_B:PCBM (circles) solar cells, made with a comparable thickness of the active layer (around 100 nm). The light power intensity is 100 mW cm^{-2}. Error bars represent standard deviations.

different dependence of V_{oc} with the light intensity (P_{in}) should be observed [33]. As an example, the variation of V_{oc} with P_{in}, for cells made with the two different donor samples and with a D:A ratio of 1:1, is displayed in the semi-logarithmic plot of Fig. 6, which shows that the dependence on light intensity was found to be much stronger in the case of PFB-co-FT_A, mainly at low P_{in}. This could be explained by considering trap-assisted recombination

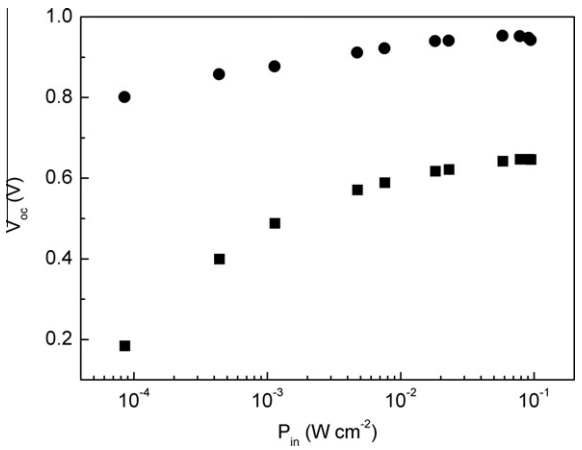

Fig. 6. Dependence of the open-circuit voltage on light power intensity for a PFB-co-FT_A: PCBM (squares) and a PFB-co-FT_B:PCBM (circles) solar cell, both made with a donor to acceptor weight ratio of 1:1 and an active layer thickness of about 100 nm.

of charge carriers [34], more relevant in the presence of high content of impurities, as also confirmed by light induced ESR and TRESR analysis.

Light induced ESR spectroscopy is frequently used to identify the occurrence of photoinduced electron transfer from conjugated polymers to fullerene, by unambiguously revealing the presence and steady state concentration of photoexcited charge-separated states (radical ions) [35–37], the signal intensity being determined by the equilibrium between photogeneration and recombination. Note however that, using the 100 kHz modulation technique, the ESR signal is mainly due to relatively long-lived radical species, with lifetimes exceeding 10 ms and with a greater sensitivity for species having lifetimes exceeding milliseconds [38]. In addition, in order to have enough signal intensity, the ESR measurements are performed at low temperature, at which not only magnetic disorder is reduced but also most of the recombination processes are severely slowed down, so that charge lifetime is increased with respect to high temperature and part of the species rapidly recombining at room temperature is brought to detection. On the other hand, time-resolved ESR techniques are frequently used to investigate, in the microsecond time range, the dynamics of formation and decay of short-lived photoexcited paramagnetic states such as triplet states and fast decaying radicals species [39]. The light induced ESR spectra of PFB-co-FT:PCBM blends, recorded at low temperature (T = 110 K), are reported in Fig. 7a. The lines in the spectra of Fig. 7a are assigned to the radical cations of PFB-co-FT and to the radical anions of PCBM, on the basis of the

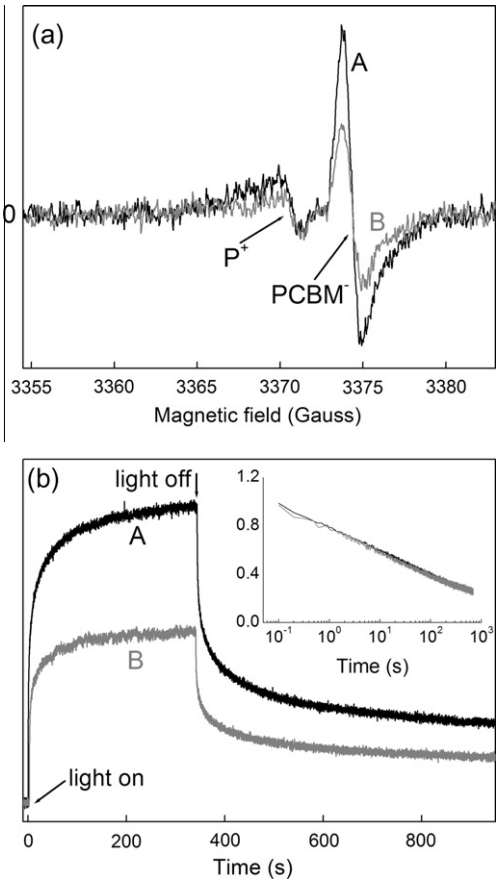

Fig. 7. (a) Light induced ESR spectra of PFB-co-FT:PCBM blends, recorded at $T = 110$ K using visible light illumination (at 488 and 514 nm with an Argon Neon laser) and 0.05 mW microwave power. (b) Onset and decay of the PCBM anion signal. Inset: signal decay normalized to 1, showing the same time dependence in both cases. A and B represent PFB-co-FT_A:PCBM and PFB-co-FT_B:PCBM blends, respectively.

g-tensor principal values estimated by a best fit simulation of the spectra ($g_x = 2.0035$, $g_y = 2.0020$, $g_z = 2.0010$ for the broader, low field line and $g_x = 2.0005$, $g_y = 1.9999$, $g_z = 1.9998$ for the high-field line, all g-values given with an absolute error of ±0.0005) [23,40].

The spectral simulation is reported in the Supplementary Data. A small difference between our g-values for PCBM and the reported values of Ref. [40], could be ascribed to matrix effects (different polymers), slightly changing the electron distribution in the anion.

The slightly lower intensity of the lines assigned to PFB-co-FT radical cations (polarons) is due to a well known saturation phenomenon already described in other polymer:PCBM blends [36,41,42]. By examining the total intensities of the ESR spectra shown in Fig. 7a, it is clear that the PFB-co-FT_A:PCBM blend shows an intensity about twice that of the blend with less Pd impurities. The different intensities could be caused either by a different efficiency of the charge generation process or by a different average lifetime of the charge carriers. Concerning the first possibility, the low concentration of impurities in the investigated PFB-co-FT samples (in the ppm range, see Table 1) cannot produce a dramatic effect on charge separation yield (the blend morphology should not be significantly affected by the residual catalyst). Moreover, we did not observe any difference in the polaron lines of PFB-co-FT:PCBM blends in a microsecond time-scale, as evidenced by the TRESR analysis (*vide infra*). On the other hand, a higher light induced ESR intensity is expected in the blend with a higher content of residual catalyst, generating a higher number of defect sites where charge carriers can be trapped and can survive for a longer time before recombination, as also inferred from TOF and solar cells results.

The different intensities of the light induced ESR spectra of Fig. 7a were attributed to a different average lifetime of the photogenerated charge carriers, however the question is if the incremented stationary state population of trapped charges observed for PFB-co-FT_A:PCBM blend is due to an increased trap concentration or to an increased trap binding energy. In order to ascertain this, the signal kinetics was registered for both blends. The formation and decay kinetics of the PCBM anion signal is reported in Fig. 7b (due to the weakness and broadness of the polaron signal, it was not possible to measure its kinetics). After switching off the illumination, the ESR signal decays slowly within the first 10 min to an almost constant value (persistent signal), without reaching the value observed before illuminating (which is almost zero). The signal decay is obviously due to the recombination of PCBM anions with oppositely charged species, that is trapped charges that can be thermally detrapped at the measuring temperature, so that can reach the transport level, diffuse and recombine. The persistent signal is instead due to charges at very deep traps, with respect to thermal energy, where they are seized over hours. As it occurs with the LESR, also in the persistent signal the intensity is higher in sample A than in sample B, that means that also deep traps are more concentrated in sample A than in B (the intensity ratio is exactly the same as in presence of light, about two). More, the time dependence of the signal normalized to 1 is exactly the same in the two samples, as shown in the inset of Fig. 7b. The observed full coincidence of the time dependence of signal kinetics suggests that the residual Pd catalyst does not affect the energy distribution of traps, but simply their concentration, being higher for PFB-co-FT_A:PCBM blend.

Time-resolved ESR spectra of PFB-co-FT:PCBM blends, recorded at $T = 120$ K and 1 μs after the laser pulse, are shown in Fig. 8. The observed TRESR spectra extend over about 200 Gauss, with a pattern in absorption at low field and emission at high field. The TRESR spectra of the investigated blends are coincident with that of PCBM dissolved in an inert solid matrix (e.g. frozen toluene or 1,2-dichlorobenzene), assigned to the excited triplet state of fullerene [43,44], but different from the spectrum of neat PCBM films, where intermolecular interactions induce fast spin relaxation and efficient decay of triplet excitons. Therefore TRESR spectra of PFB-co-FT:PCBM blends are attributed to the triplet state of isolated fullerene molecules in the polymer matrix, not to fullerene aggregates. According to this fact, the PCBM triplet state can be considered as a probe of the charge carrier dynamics of the PFB-co-FT matrix in which it is embedded. It is worth noting that in the centre of the TRESR spectra (at $g = 2$, corresponding to a magnetic

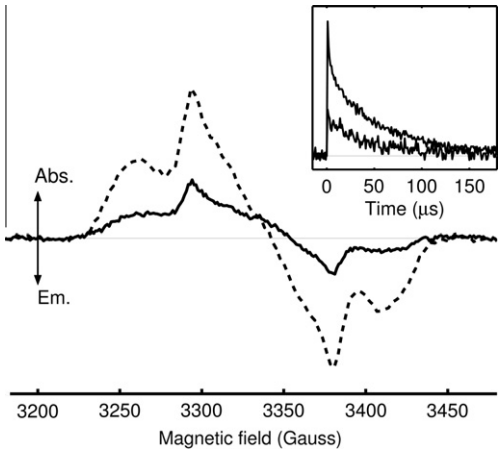

Fig. 8. TRESR spectra of PFB-co-FT:PCBM blends at 120 K, recorded 1 μs after the laser pulse with 2 mW microwave power (Abs. = absorption; Em. = emission). Dashed line: PFB-co-FT_A:PCBM; continuous line: PFB-co-FT_B:PCBM. Inset: Decay of the TRESR signals, recorded at the field position corresponding to the maximum ESR intensity and using very low microwave power (2 μW).

field of 3345 Gauss in Fig. 8), there are very weak signals that can be attributed to the radical pairs formed by photo-induced charge transfer. Even though no quantitative conclusion can be drawn from these spectra, by observing the $g \sim 2$ region with an increased signal to noise, the intensities of polaron lines always do not differ significantly in the two blends (within experimental errors), giving support to the assumption of a comparable charge photogeneration yield. The fraction of 532 nm light absorbed by the copolymer in PFB-co-FT:PCBM blends produces charge separated states, but this is not the main process, because of the poor absorption ability of PFB-co-FT at this wavelength (see Supplementary Data, Fig. S3). Indeed, the 532 nm light is also absorbed by PCBM, generating singlet excited states (singlet excitons) efficiently converted into a triplet states and giving rise to the triplet species detected by TRESR. The catalyst impurities in PFB-co-FT_A cannot significantly increase the PCBM triplet generation, because the triplet quantum yield in [60] fullerene and its derivatives is usually already close to unity [45]. Despite this, the TRESR spectrum obtained from PFB-co-FT_A:PCBM blend is about two-fold more intense than that of PFB-co-FT_B:PCBM. This result, confirmed by repeated measurements on at least three independent samples, can be explained by considering the different density of trap states of polarons in the blends with low residual catalyst content. After pulsed photoexcitation with high photon flux, corresponding to our experimental conditions, a large number of charge carriers are generated. In the presence of an excess of charge carriers, all trap sites are filled and additional free carriers are generated at the mobility edge. The free carriers undergo a fast bimolecular quenching within less than 100 ns [46]. Freely diffusing polarons are also able to quench excited triplet states, as recently demonstrated in polymer/chromophore blends [47]. Therefore, it could be suggested that, because of the higher number of free polarons in PFB-co-FT_B (due to the low density of trap states), the probability of polaron-triplet exciton encounter is enhanced, thus leading to a more efficient triplet quenching within the first few tens of nanoseconds. The higher density of mobile polarons in PFB-co-FT_B could in principle give rise also to a variation of triplet PCBM lineshape because of an enhancement of relaxation rates. However we did not observe a significant TREPR linewidth change between the two samples and the lineshape is almost coincident with that of triplet PCBM in an inert matrix (e.g. frozen dichlorobenzene solution). The time resolution of TRESR in our experimental setup is more than 100 ns. Therefore the fast quenching of triplet states in PFB-co-FT_B causes the decreased intensity of TRESR spectrum measured at about 1 ms after the laser pulse. The annihilation of triplet states by polarons is most effective during the first 100 ns but can be present also at a longer time scale. In order to check whether this is true, we measured the TRESR decay curve in a 100 μs time range on the two blends and determined the decay constant of the curves (inset of Fig. 8). The best fit of the TRESR signal decay, using a monoexponential function, yielded the average decay times of 52 ± 3 μs and 38 ± 5 μs for PFB-co-FT_A:PCBM and PFB-co-FT_B:PCBM blend, respectively. An example of two decay curves with their fittings is reported in the Supplementary Data. The shorter decay time of the triplet state in latter blend is an evidence in favour of an additional decay process, besides the normal unimolecular triplet decay, likely induced by an increased triplet-polaron quenching in the blend with a higher number of available mobile polarons, in agreement with previous evidences from electrical characterization.

4. Conclusions

The effect of residual Pd catalyst on transport properties of PFB-co-FT, as well as on the photovoltaic and photophysical behavior of PFB-co-FT:PCBM blends were investigated. The residual catalyst impurities were the result of the polymerization/purification process and not intentionally added to the investigated copolymer samples.

As expected, higher hole mobilities were measured for the PFB-co-FT sample with a lower impurity content. Moreover, the dependence of transit times on the electric field indicated a higher dispersion character for the transport of positive carriers in the Pd-rich copolymer sample, attributed to a higher density of trap states.

Open-circuit voltage and fill factor were the photovoltaic parameters mainly affected by the residual Pd catalyst, showing higher values for cells made with the donor sample with a higher purity and leading to an increased power conversion efficiency of around twice. The analysis of the trend of the open-circuit voltage with light intensity confirmed a stronger trapping effect for cells made with the PFB-co-FT sample richer of residual catalyst impurities.

Evidences of increased charge trapping in PFB-co-FT:PCBM blends made from the copolymer with a higher impurity level were also provided by light induced ESR analysis, showing an increased stationary state signal of trapped charges with respect to the purer PFB-co-FT sample. At the same time, in time-resolved ESR analysis the faster decay of photoexcited PCBM triplet state in the purer

blend points to a more effective triplet-polaron quench, in agreement with a higher average polaron mobility. For the first time, the PCBM molecule in triplet state is here employed as a probe of the polymeric environment.

In conclusion, all the different experimental evidences point to a common effect of higher density of trap states in the copolymer sample with a higher content of the residual palladium catalyst, greatly affecting the photovoltaic performance of the related solar cells.

Acknowledgements

The authors thank S. Perucchini for elemental analysis, A. Tacca for electrochemical measurements, N. Perin for spectroscopic characterization, S. Spera for NMR analysis and A. Oldani for molecular weights measurements. NC, AT, MR and LF acknowledge financial support for this work by ENI S.p.A. (Contract Nos. 4700007315 and 3500001635), by Italian MIUR (PRIN20085M27SS) and by University of Padova (CPDA085989).

Appendix A. Supplementary data

Supplementary data associated with this article can be found, in the online version, at doi:10.1016/j.orgel.2011.12.005.

References

[1] G. Dennler, M.C. Scharber, C.J. Brabec, Polymer–fullerene bulk-heterojunction solar cells, Advanced Materials 21 (2009) 1323–1338.
[2] J. Chen, Y. Cao, Development of novel conjugated donor polymers for high-efficiency bulk-heterojunction photovoltaic devices, Accounts of Chemical Research 42 (2009) 1709–1718.
[3] R. Po, M. Maggini, N. Camaioni, Polymer solar cells: recent approaches and achievements, Journal of Physical Chemistry C 114 (2010) 695–706.
[4] Z. He, C. Zhong, X. Huang, W.-Y. Wong, H. Wu, L. Chen, S. Su, Y. Cao, Simultaneous enhancement of open-circuit voltage, short-circuit current density, and fill factor in polymer solar cells, Advanced Materials 23 (2011) 4636–4643.
[5] J.D. Kotlarski, D.J. D Moet, P.W.M. Blom, Role of balanced charge carrier transport in low band gap polymer:fullerene bulk heterojunction solar cells, Journal of Polymer Science B 49 (2011) 708–711.
[6] D. Mihailetchi, H. Xie, B. de Boer, L.J.A. Koster, P.W.M. Blom, Charge transport and photocurrent generation in poly(3-hexylthiophene): methanofullerene bulk-heterojunction solar cells, Advanced Functional Materials 16 (2006) 699–708.
[7] M.-H. Chen, J. Hou, Z. Hong, G. Yang, S. Sista, L.-M. Chen, Y. Yang, Efficient polymer solar cells with thin active layers based on alternating polyfluorene copolymer/fullerene bulk heterojunctions, Advanced Materials 21 (2009) 4238–4242.
[8] P.W.M. Blom, V.D. Mihailetchi, L.J.A. Koster, D.E. Markov, Device physics of polymer:fullerene bulk heterojunction solar cells, Advanced Materials 19 (2007) 1551–1566.
[9] L.J.A. Koster, V.D. Mihailetchi, P.W.M. Blom, Bimolecular recombination in polymer/fullerene bulk heterojunction solar cells, Applied Physics Letters 88 (2006) 052104.
[10] C.J. Brabec, S.E. Shaheen, T. Fromherz, F. Padinger, J.C. Hummelen, A. Dhanabalan, R.A.J. Janssen, N.S. Sariciftci, Organic photovoltaic devices produced from conjugated polymer/methanofullerene bulk heterojunctions, Synthetic Metals 121 (2001) 1517–1520.
[11] V. Coropceanu, J. Cornil, D.A. da Silva Filho, Y. Olivier, R. Silbey, J.L. Brédas, Charge transport in organic semiconductors, Chemical Reviews 107 (2007) 926–952.
[12] M. Jaiswal, R. Menon, Polymer electronic materials: a review of charge transport, Polymer International 55 (2006) 1371–1384.
[13] Y.-J. Cheng, S.-H. Yang, C.-S. Hsu, Synthesis of conjugated polymers for organic solar cell applications, Chemical Reviews 109 (2009) 5868–5923.
[14] F.C. Krebs, R.B. Nyberg, M. Jorgensen, Influence of residual catalyst on the properties of conjugated polyphenylenevinylene materials: palladium nanoparticles and poor electrical performance, Chemistry of Materials 16 (2004) 1313–1318.
[15] Z. Bao, Y. Chen, R. Cai, L. Yu, Conjugated liquid-crystalline polymers – soluble and fusible poly(phenylenevinylene) by the Heck coupling reaction, Macromolecules 26 (1993) 5281–5286.
[16] M.S.A. Abdou, X. Lu, Z.W. Xie, F. Orfino, M.J. Deen, S. Holdcroft, Nature of impurities in π-conjugated polymers prepared by ferric chloride and their effect on the electrical properties of metal–insulator–semiconductor structures, Chemistry of Materials 7 (1995) 631–641.
[17] P. Sonar, A.C. Grimsdale, M. Heeney, M. Shkunov, I. McCulloch, K. Müllen, A study of the effects metal residues in poly(9,9-dioctylfluorene) have on field-effect transistor device characteristics, Synthetic Metals 157 (2007) 872–875.
[18] N. Björklund, J.-O. Lill, J. Rajander, R. Österbacka, S. Tierney, M. Heeney, I. McCulloch, M. Cölle, The effects of metal impurities in poly[(2,5-bis(3-decylthiophen-2-yl)-thieno[2,3-b]thiophene] on field-effect transistor properties, Organic Electronics 10 (2009) 215–221.
[19] P.A. Troshin, D.K. Susarova, Y.L. Moskvin, I.E. Kuznetsov, S.A. Ponomarenko, E.N. Myshkovskaya, K.A. Zakharcheva, A.A. Balakai, S.D. Babenko, V.F. Razumov, Impedance measurements as a simple tool to control the quality of conjugated polymers designed for photovoltaic applications, Advanced Functional Materials 20 (2010) 4351–4357.
[20] A. Saeki, M. Tsuji, S. Seki, Direct evaluation of intrinsic optoelectronic performance of organic photovoltaic cells with minimizing impurities and degradation effect, Advanced Energy Materials 1 (2011) 661–669.
[21] I.F. Perepichka, D.F. Perepichka, Handbook of Thiophene-Based Materials, vol. 1, Wiley, Chichester, 2009.
[22] J. Kettle, M. Horie, L.A. Majewski, B.R. Saunders, S. Tuladhar, J. Nelson, M.L. Turner, Optimization of PCPDTBT solar cells using polymer synthesis with Suzuki coupling, Solar Energy Materials and Solar Cells 95 (2011) 2186–2193.
[23] L. Bonoldi, A. Calabrese, A. Pellegrino, N. Perin, R. Po, S. Spera, A. Tacca, Optical and electronic properties of fluorene/thiophene/benzothiadiazole pseudorandom copolymers for photovoltaic applications, Journal of Material Science 46 (2011) 3960–3968.
[24] M. Pope, C.E. Swenberg, Electronic Processes in Organic Crystals and Polymers, second ed., Oxford University Press, New York, 1999.
[25] F. Laquai, G. Wegner, C. Im, H. Bässler, S. Heun, Nondispersive hole transport in carbazole- and anthracene-containing polyspirobifluorene copolymers studied by the charge-generation layer time-of-flight technique, Journal of Applied Physics 99 (2006) 033710.
[26] W.Y. Hung, T.H. Ke, Y.T. Lin, C.C. Wu, T.H. Hung, T.C. Chao, K.T. Wong, C.I. Wu, Employing ambipolar oligofluorene as the charge-generation layer in time-of-flight mobility measurements of organic thin films, Applied Physics Letters 88 (2006) 064102.
[27] H.H. Poole, On the dielectric constant and electrical conductivity of mica in intense field, Philosophical Magazine 32 (1916) 112–129.
[28] J. Frenkel, On pre-breakdown phenomena in insulators and electronic semi-conductors, Physical Reviews 54 (1938) 647–648.
[29] P.M. Borsenberger, D.S. Weiss, Organic Photoreceptors for Xerography, Marcel Dekker, New York, 1998.
[30] T. Tiedje, A. Rose, A physical interpretation of dispersive transport in disordered semiconductors, Solid State Communications 37 (1981) 49–52.
[31] H. Scher, E.W. Montroll, Anomalous transit-time dispersion in amorphous solids, Physical Reviews B 12 (1975) 2455–2477.
[32] C.J. Brabec, A. Cravino, D. Meissner, N.S. Sariciftci, T. Fromherz, M.T. Rispens, L. Sanchez, J.C. Hummelen, Origin of the open circuit voltage of plastic solar cells, Advanced Functional Materials 11 (2001) 374–380.
[33] M.M. Mandoc, F.B. Kooistra, J.C. Hummelen, B. de Boer, P.W.M. Blom, Effect of traps on the performance of bulk heterojunctions organic solar cells, Applied Physics Letters 91 (2007) 263505.
[34] M.M. Mandoc, W. Veurman, L.J.A. Koster, B. de Boer, P.W.M. Blom, Origin of the reduced fill factor and photocurrent in MDMO-PPV:PCNEPV all-polymer solar cells, Advanced Functional Materials 17 (2007) 2167–2173.
[35] V. Dyakonov, G. Zoriniants, M. Scharber, C.J. Brabec, R.A.J. Janssen, J.C. Hummelen, N.S. Sariciftci, Photoinduced charge carriers in

conjugated polymer–fullerene composites studied with light-induced electron-spin resonance, Physical Reviews B 59 (1999) 8019–8025.
[36] V. Dyakonov, D. Godovsky, J. Parisi, C.J. Brabec, N.S. Sariciftci, J.C. Hummelen, J. De Ceuster, E. Goovaerts, Spectroscopy on polymer–fullerene composites and photovoltaic cells, Synthetic Metals 121 (2001) 1529–1532.
[37] A. Aguirre, P. Gast, S. Orlinskii, I. Akimoto, E.J.J. Groenen, H. El Mkami, E. Goovaerts, S. Van Doorslaer, Multifrequency EPR analysis of the positive polaron in I2-doped poly(3-hexylthiophene) and in poly[2-methoxy-5-(3,7-dimethyloctyloxy)]-1,4-phenylenevinylene, Physical Chemistry Chemical Physics 10 (2008) 7129–7138.
[38] M.D. Heinemann, K. Von Maydell, F. Zutz, J. Kolny-Olesiak, H. Borchert, I. Riedel, J. Parisi, Photo-induced charge transfer and relaxation of persistent charge carriers in polymer/nanocrystal composites for applications in hybrid solar cells, Advanced Functional Materials 19 (2009) 3788–3795.
[39] N. Hirota, S. Yamauchi, Short-lived excited triplet states studied by time-resolved EPR spectroscopy, Journal of Photochemistry and Photobiology, C: Photochemistry Reviews 4 (2003) 109–124.
[40] J. De Ceuster, E. Goovaerts, A. Bouwen, J.C. Hummelen, V. Dyakonov, High-frequency (95 GHz) electron paramagnetic resonance study of the photoinduced charge transfer in conjugated polymer–fullerene composites, Physics Reviews B 64 (2001) 195206–195211.
[41] K. Marumoto, N. Takeuchi, T. Ozaki, S. Kuroda, ESR studies of photogenerated polarons in regioregular poly(3-alkylthiophene)–fullerene composite, Synthetic Metals 129 (2002) 239–247.
[42] V.I. Krinichnyi, H.K. Roth, S. Sensfuss, M. Schrodner, M. Al-Ibrahim, Dynamics of photoinduced radical pairs in poly(3-dodecylthiophene)/fullerene composite, Physica E: Low-dimensional Systems and Nanostructures 36 (2007) 98–101.
[43] L. Pasimeni, U. Segre, M. Ruzzi, M. Maggini, M. Prato, K. Kordatos, Preferential orientation of fulleropyrrolidine bisadducts in E7 liquid crystal: a time-resolved electron paramagnetic resonance study, Journal of Physical Chemistry B 103 (1999) 11275–11281.
[44] G. Agostini, C. Corvaja, M. Maggini, L. Pasimeni, M. Prato, Fullerene derivatives in poly(methyl methacrylate): an EPR and zero-field ODMR study of their photoexcited triplet states, Journal of Physical Chemistry 100 (1996) 13416–13420.
[45] A. Hirsch, M. Brettreich, Fullerenes, Chemistry and Reactions, Wiley-VCH, Weinheim, 2005.
[46] I. Montanari, A.F. Nogueira, J. Nelson, J.R. Durrant, C. Winder, M.A. Loi, N.S. Sariciftci, C.J. Brabec, Transient optical studies of charge recombination dynamics in a polymer/fullerene composite at room temperature, Applied Physics Letters 81 (2002) 3001–3003.
[47] D. Hertel, K. Meerholz, Triplet-polaron quenching in conjugated polymers, Journal of Physical Chemistry B 111 (2007) 12075–12080.